Inverse Klein tunneling effect in binary waveguide arrays

Minh C. Tran [1,2,3,*] Quang Nguyen-The [4] Cuong C. Do,[5] and Truong X. Tran [6,†]

[1]*Atomic Molecular and Optical Physics Research Group, Science and Technology Advanced Institute, Van Lang University, 69/68 Dang Thuy Tram street, 70000 Ho Chi Minh city, Vietnam*

[2]*Faculty of Technology, Van Lang University, 69/68 Dang Thuy Tram street, 70000 Ho Chi Minh city, Vietnam*

[3]*Nuclear Training Center, VINATOM, 140 Nguyen Tuan street, 10000 Ha Noi, Vietnam*

[4]*Department of Communications, Le Quy Don Technical University, 236 Hoang Quoc Viet street, 10000 Hanoi, Vietnam*

[5]*Institute for Nuclear Science and Technology, VINATOM, 179 Hoang Quoc Viet street, 10000 Ha Noi, Vietnam*

[6]*Department of Physics, Le Quy Don Technical University, 236 Hoang Quoc Viet street, 10000 Hanoi, Vietnam*

(Received 29 November 2021; accepted 14 February 2022; published 25 February 2022)

We have systematically investigated the optical analog of the inverse Klein tunneling effect—a quantum relativistic effect emerging from the Dirac equation and that is inverse to the well-known Klein tunneling effect. Inverse Klein tunneling can be observed if an electron moves through an inverse potential step from one region with high potential into the adjacent region with low potential. We propose to mimic this effect by launching a Dirac soliton around Dirac points in binary waveguide arrays where the inverse potential step can be easily created by introducing an offset for refractive indices of the waveguides. We obtain the analytical formulas for the transmission coefficient of a plane wave through the inverse potential step in the discrete model with binary waveguide arrays and in the continuous model. As expected, around the Dirac points these two theoretical results are in good agreement. We also show that the theoretical transmission coefficient in binary waveguide arrays is in excellent agreement with the numerical results obtained directly via the beam propagation simulation method. This verification confirms the validity of our model and theoretical results on inverse Klein tunneling in binary waveguide arrays. Some important relations for the transmission coefficient while comparing the inverse Klein tunneling effect and the Klein tunneling effect are also provided.

DOI: 10.1103/PhysRevA.105.023523

I. INTRODUCTION

Waveguide arrays (WAs) possess many remarkable discrete photonic phenomena, e.g., discrete diffraction [1,2], discrete solitons [1,3–5], the emission of the diffractive resonant radiation from discrete solitons [6], discrete solitons' self-wave-number shift [7], and the supercontinuum in both frequency and wave number domains [8].

Waveguide arrays have also been intensively explored for mimicking fundamental nonrelativistic quantum mechanics effects arising from the Schrödinger equation, for example, Bloch oscillations [1,9,10] and Zener tunneling [11]. On the other hand, binary waveguide arrays (BWAs)—a special class of WAs formed by two different alternating types of waveguides—are a wonderful photonic system to investigate fundamental relativistic quantum mechanics phenomena emerging from the Dirac equation, for instance, *Zitterbewegung* [12] and Dirac solitons (DSs) in both one-dimensional [13–15] and two-dimensional cases [16]. Moreover, by changing the propagation mismatch parameter in BWAs along the longitudinal axis, one can obtain the Dirac equation in curved space-time with variable mass [17]. Quite recently, it has been shown that in BWAs with curved space-time one can observe the spontaneous symmetry breaking of DSs and switch an intense DS by using an extremely weak signal at the input [18].

Recently, it has been shown that at the interface of two BWAs having opposite signs of the Dirac mass one can generate the optical analog of a special state, well known in quantum field theory as a *Jackiw-Rebbi* (JR) solution [19], both in the linear regime [20] and the nonlinear regime [21]. The interaction between DSs and JR states in BWAs has been analyzed in Ref. [22]. Based on JR states, the fundamental charge fractionalization phenomenon (which has a fundamental role in the fractional quantum Hall effect) was predicted [23]. The JR state is also well known for the topological nature of its zero-energy solution which is a precursor to topological insulators [24]. Topological photonics has great potential in the development of extremely robust optical circuits [25]. As expected, the JR states in BWAs also possess extreme robustness under the influence of very strong disturbances [26]. The JR states and trivial states both found in interfaced BWAs practically do not interact with each other at all, even if they are located very close to each other [27]. This amazing feature can be exploited to reliably guide optical signals in a network where many channels of different types are tightly distributed. On the contrary, two JR states (or two trivial states) in interfaced BWAs can strongly couple to each other in the linear regime and possess the switching effect in the nonlinear regime like in fiber couplers [27].

Another peculiar fundamental quantum relativistic effect called Klein tunneling has also been investigated in BWAs

*trancongminh@vlu.edu.vn

†Corresponding author: tranxtr@gmail.com

both theoretically [28] and experimentally [29]. Klein tunneling (KT) was predicted by Klein in 1929 [30]; he theorized that relativistic fermions can tunnel through large repulsive potential steps, which are higher than the energy of the particle, without the exponential decaying expected in quantum nonrelativistic tunneling processes governed by the well-known Schrödinger equation. This amazing phenomenon is due to the existence of negative-energy solutions of the Dirac equation [31]. However, because of its very high field requirement, KT for relativistic electrons has not been demonstrated experimentally yet. In addition, the potential step must be sufficiently steep in order for KT to be observed [32]; i.e., it must occur at a very narrow region which is comparable or shorter than the Compton wavelength. Otherwise, it becomes practically impenetrable for relativistic electrons as in nonrelativistic tunneling theory. Because KT is all based in the Dirac equation, one can observe the analogs of KT in systems with linear dispersion relations similar to those of relativistic electrons described by a Dirac evolution equation. For example, in graphene the energy dispersion relation possesses a linear slope; therefore, charge carriers can show the KT [33–36]. Consequently, evidence of KT has been experimentally demonstrated in graphene [37,38], in carbon nanotubes [39], and by using cold ions in an optical trap [40]. It has also been shown in Ref. [40] that KT is a wave phenomenon and, thus, can be mimicked in a classical system which is generally much simpler than quantum systems in terms of experimental implementation. As a result, several optical schemes have been used to directly observe KT by propagation of light beams in systems of coupled waveguides, for example, in 2D honeycomb photonic lattices [41] and in planar BWAs by launching a Gaussian beam at the input [28,29]. Quite recently, KT in planar BWAs has been investigated also in planar BWAs but by launching a DS at the input [42]. The DS is a great candidate for exploring KT, because it can propagate in BWAs, conserving quite well its shape and profile during evolution.

In this work, inspired by the earlier achievements in investigating KT in BWAs, we study the inverse KT effect which is literally *inverse* to the KT effect. For observing KT in BWAs, one launches an incident beam belonging to the *positive* branch (or electron branch) of the dispersion relation so that it hits the potential step and generates the transmitted beam belonging to the *negative* branch (or positron branch). Inversely, to observe the inverse KT effect, we now propose to launch an incident beam belonging to the *negative* branch which hits the *inverse* potential step and generates the transmitted beam belonging to the *positive* branch. So, these two processes (KT and inverse KT) can be combined together to help us analyze the situation where a particle (or a beam) hits and tunnels through a rectangular potential barrier; the results of this analysis will be published elsewhere. The paper is organized as follows. In Sec. II we summarize the theoretical results obtained in Refs. [28,42] for the KT effect. In Section. III we provide the analytical formulas for the inverse KT effect. In Sec. IV we verify these theoretical results for the KT in BWAs by comparing them with the results obtained by the beam propagation method. Finally, in Sec. V we summarize our results and finish with concluding remarks.

II. KLEIN TUNNELING EFFECT IN BINARY WAVEGUIDE ARRAYS: TRANSMISSION OF LINEAR PLANE WAVES THROUGH A POTENTIAL STEP

To start with, let us briefly reintroduce the optical analog of the Klein tunneling effect in BWAs where a plane wave transmits through a potential step. The theoretical background in this section is needed for further discussion about the inverse KT effect. Light propagation in a BWA with Kerr nonlinearity can be described, in the continuous-wave regime, by the following dimensionless coupled-mode equation [3,29,42,43]:

$$i\frac{da_n}{dz} = -\beta_n a_n - \kappa[a_{n+1} + a_{n-1}] + (-1)^n \sigma a_n - \gamma |a_n|^2 a_n, \tag{1}$$

where a_n is the electric field amplitude in the waveguide with position n; z is the longitudinal spatial coordinate; 2σ and κ are the propagation mismatch and the coupling coefficient between two adjacent waveguides of the array, respectively; and γ is the nonlinear coefficient of the waveguides. As in Ref. [29], the quantity β_n is needed to create an offset in propagation constants for waveguides which is necessary for mimicking the potential step required for KT and is defined as $\beta_n = 0$ for all waveguides with $n < 0$ (region I) and $\beta_n = \beta_0$ for all waveguides with $n \geqslant 0$ (region II) [see Fig. 1(b)]. So, as seen from Eq. (1), the quantity $[\beta_n - (-1)^n\sigma]$ characterizes the propagation constant of the nth waveguide of the BWA whose transverse refractive index profile is schematically illustrated in Fig. 1(c). In the case of focusing nonlinearity, in general, in the dimensionless form one can normalize variables in the above equation such that both γ and κ are equal to unity.

When a beam is launched into BWAs around the so-called Bragg angles which correspond to the central spatial wave number of the beam $Q_B = \pm\pi/2$ [12], one can set $\Psi_1(n) = (-1)^n a_{2n}$ and $\Psi_2(n) = i(-1)^n a_{2n-1}$. Then by following the standard approach developed in Refs. [12,44], one can introduce the continuous transverse coordinate $\xi \leftrightarrow n$ and the two-component spinor $\Psi(\xi, z) = (\Psi_1, \Psi_2)^T$ which lead to the one-dimensional nonlinear Dirac equation [13,29,42]:

$$i\partial_z \Psi = V(\xi)\Psi - i\kappa\hat{\sigma}_x\partial_\xi\Psi + \sigma\hat{\sigma}_z\Psi - \gamma G, \tag{2}$$

where the nonlinear term $G \equiv (|\Psi_1|^2\Psi_1, |\Psi_2|^2\Psi_2)^T$, and $\hat{\sigma}_x$ and $\hat{\sigma}_z$ are the usual Pauli matrices. The potential step $V(\xi) = 0$ for $\xi < 0$ and $V(\xi) = \Phi_0 = -\beta_0 > 0$ for $\xi \geqslant 0$ [see Fig. 1(a)]. Without the nonlinear term, Eq. (2) is exactly the same as Eq. (4) in Ref. [28], which is the well-known one-dimensional Dirac equation for the two-component spinor Ψ of a relativistic particle in the potential V where z and ξ in Eq. (2) play the roles of the temporal t and the spatial variables x, respectively (see Eq. (1) in Ref. [29]). Note that to mimic the positive potential step $V(\xi)$ in the Dirac equation (2) and shown in Fig. 1(a), the array β_n in Eq. (1) must have the profile as shown in Fig. 1(b), i.e., the parameter β_0 must be negative.

The transmission coefficient T for the KT effect of a plane wave through the potential step was derived based on Eq. (1) in the linear regime in Ref. [28]. In the rest of this section we reintroduce the main results obtained in Refs. [28,42] for T. For now, we just ignore the potential step and suppose that the

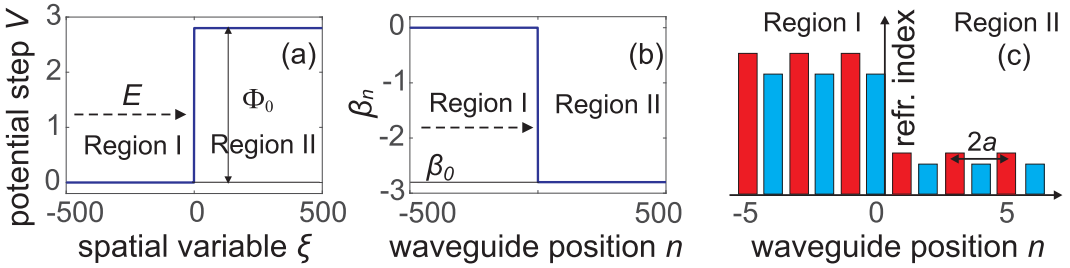

FIG. 1. (a) Scheme for investigating the Klein tunneling effect of a particle with energy E through a potential step $V(\xi)$ with potential height $\Phi_0 > E$. (b) Propagation constant offset β_n introduced to a BWA to mimic the potential step $V(\xi)$. (c) Transverse refractive index profile of the BWA. This figure is reproduced from Fig. 1 in Ref. [42].

array β_n is independent of n and $\beta_n = \beta = -\Phi$, and then by making the following Ansatz of a *plane-wave* traveling in the plane (n, z) under some inclination,

$$a_n(Q) \sim \exp[i(Qn - \omega z)], \tag{3}$$

one can show that the discrete coupled-mode Eq. (1) supports two minibands whose dispersion curves obey the following relations (see Ref. [43]):

$$\omega_{\pm}(Q, \Phi) = \Phi \pm \sqrt{\sigma^2 + 4\kappa^2 \cos^2 Q}, \tag{4}$$

where Q is the normalized wave number of the plane wave which is equivalent to the quantity qa in Eq. (3) in Ref. [28], with a being the center-to-center distance between two adjacent waveguides in BWAs, and q is the wave number of the plane wave. The normalized wave number Q represents the phase difference between two adjacent waveguides. Parameter ω can be interpreted as the energy (or frequency) of the plane wave if we recall the following transformations: $n \to \xi \to x$ and $z \to t$. The dispersion relation curves $\omega_{\pm}$ as functions of the wave number Q are plotted in Fig. 2(a), where the left panel with solid curves represents the case with $\Phi = 0$ (i.e., region I in Fig. 1), and the right panel with dashed curves represents the case with $\Phi = \Phi_0$ (i.e., region II in Fig. 1). The two upper curves in Fig. 2(a) represent the so-called positive-energy branch ω_+ (also known as the electron

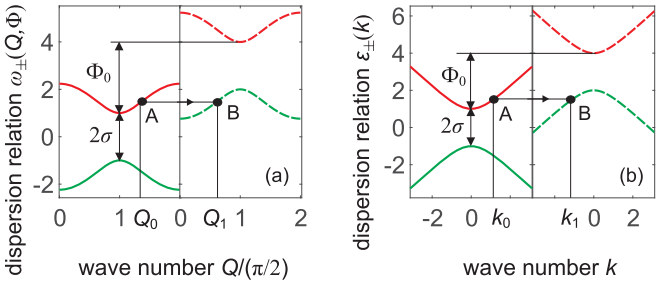

FIG. 2. (a) Dispersion relation curves $\omega_{\pm}(Q, \Phi)$ when $\Phi = 0$ (solid curves) and $\Phi = \Phi_0$ (dashed curves) based on Eq. (4) for explaining the physical mechanism of the KT effect in BWAs in the linear regime. (b) Dispersion relation curves $\epsilon_{\pm}(k, \Phi)$ when $\Phi = 0$ (solid curves) and $\Phi = \Phi_0$ (dashed curves) based on Eq. (5) for explaining the physical mechanism of the KT effect with the continuous model in the linear regime.

branch), whereas the two lower curves therein represent the negative-energy (or positron) branch ω_-.

The dispersion relations in the form of Eq. (4) are obtained based on the discrete coupled-mode Eq. (1). Similarly, by making the ansatz $\Psi \sim \exp[i(k\xi - \epsilon z)$ for the continuous *linear* Eq. (2) (i.e., when $\gamma = 0$) with uniform potential Φ, one can obtain two branches for positive- and negative-energy states of the free relativistic electron (see Eq. (6) in Ref. [28]):

$$\epsilon_{\pm}(k, \Phi) = \Phi \pm \sqrt{\sigma^2 + \kappa^2 k^2}. \tag{5}$$

In the same way as in Fig. 2(a), the dispersion curves ϵ_+ and ϵ_- based on Eq. (5) are plotted in Fig. 2(b) for the cases with $\Phi = 0$ (left panel) and $\Phi = \Phi_0$ (right panel).

If the normalized wave number is written as $Q = \pm\pi/2 + k/2$ when k is small enough, then one can easily see that Eq. (4) is an approximate version of Eq. (5). So, now one can be sure that if the beam travels in the BWA around the Bragg angles of inclination, i.e., if $Q \simeq \pm\pi/2$, then Eq. (1) can be transformed into the Dirac Eq. (2).

If an incident plane wave [illustrated by point A in Fig. 2(a)] belongs to the upper curve ω_+ of the BWA traveling in region I and has the incident wave number $Q_0 = \pi/2 + k_0/2$ with $0 < k_0 < \pi$, then this plane wave will hit the potential step with the height $\Phi_0 = -\beta_0$. If Φ_0 is low enough, then the conventional damping of the transmitted wave will take place as governed by the quantum nonrelativistic Schrödinger equation. On the contrary, if the potential step is high enough, one can observe the optical analog of the KT based on Eq. (1). In this case, the transmitted wave illustrated by point B in Fig. 2(a) will be another plane wave belonging to the lower curve ω_- of the BWA traveling in region II with a certain constant amplitude (instead of decaying) and with the transmitted wave number Q_1 obtained from the energy conservation condition:

$$\omega_-(Q_1, \Phi_0) = \omega_+(Q_0, 0) \equiv \omega_0, \tag{6}$$

with the constraint $0 < Q_1 < \pi/2$ [therefore, $k_1 = 2Q_1 - \pi$ must belong to the interval $(-\pi, 0)$] to ensure a positive group velocity of the transmitted wave. The power transmission coefficient T through the potential step is calculated as follows

(see Eq. (7) in Ref. [42]):

$$T(Q_0, \Phi_0) = \frac{(\omega_0 - \sigma)(\omega_0 - \sigma - \Phi_0)\sin(2Q_0)\sin(2Q_1)}{[\Phi_0 \cos Q_0 \cos Q_1]^2 + [(\omega_0 - \sigma)\sin Q_0 \cos Q_1 + (\omega_0 - \sigma - \Phi_0)\sin Q_1 \cos Q_0]^2}. \tag{7}$$

The transmission coefficient T in the form of Eq. (7) is based on Eq. (1) for the discrete model in BWAs in the *linear* regime. The transmission coefficient T_D based on the Dirac Eq. (2) for the continuous model in the linear regime has been calculated much earlier as follows (see, for instance, Ref. [45] and Eq. (A18) in Ref. [28]):

$$T_D(k_0, \Phi_0) = 1 - \left| \frac{-k_1(\epsilon_0 - \sigma) + k_0(\epsilon_0 - \sigma - \Phi_0)}{k_1(\epsilon_0 - \sigma) + k_0(\epsilon_0 - \sigma - \Phi_0)} \right|^2, \tag{8}$$

where k_0 and k_1 are the wave numbers of the incident and transmitted plane waves, respectively, which obey the following energy conservation relation:

$$\epsilon_0 \equiv \epsilon_+(k_0, 0) = \epsilon_-(k_1, \Phi_0), \tag{9}$$

with k_0 being positive and k_1 being negative to ensure positive group velocities for both incident and transmitted plane waves. As in Fig. 2(a) for the discrete model, point A and point B in Fig. 2(b) illustrate the incident and transmitted plane waves in the continuous model, respectively. The arrow in the direction from A $\rightarrow$ B means that the incident wave (point A) generates the transmitted wave (point B).

From the dispersion relation in the form of Eq. (4) and the energy conservation law in the form of Eq. (6), the following conditions for observing the KT effect in BWAs in the linear regime have been derived in Ref. [42].

(i) If an incident plane wave hits the potential step with the incident normalized wave number $\pi/2 < Q_0 < \pi$, then the potential step height Φ_0 must satisfy the following condition (see Eq. (13) in Ref. [42]):

$$\sigma + \sqrt{\sigma^2 + 4\kappa^2 \cos^2 Q_0} < \Phi_0 < \sqrt{\sigma^2 + 4\kappa^2} + \sqrt{\sigma^2 + 4\kappa^2 \cos^2 Q_0}. \tag{10}$$

(ii) If the potential step height satisfies the condition $2\sigma < \Phi_0 < 2\sqrt{\sigma^2 + 4\kappa^2}$, then the incident wave number must satisfy the following condition (see Eq. (15) in Ref. [42]):

$$\frac{\pi}{2} < Q_0 < \text{acos}\frac{-\sqrt{\Phi_0^2 - 2\Phi_0\sigma}}{2\kappa}. \tag{11}$$

In the same way, from the dispersion relation in the form of Eq. (5) and the energy conservation law in the form of Eq. (9), the following conditions for observing the KT effect in the continuous model in the linear regime have been derived in Ref. [42].

(i) If an incident plane wave hits the potential step with the incident wave number $0 < k_0 < \pi$, then the following condition for the potential step height Φ_0 must be held true (see Eq. (14) in Ref. [42]):

$$\Phi_0 > \sigma + \sqrt{\sigma^2 + \kappa^2 k_0^2}. \tag{12}$$

(ii) If the potential step height satisfies the condition $\Phi_0 > 2\sigma$, then the incident wave number must satisfy the following condition (see Eq. (16) in Ref. [42]):

$$0 < k_0 < \frac{\sqrt{\Phi_0^2 - 2\Phi_0\sigma}}{\kappa}, \tag{13}$$

or, equivalently,

$$\frac{\pi}{2} < Q_0 < \frac{\pi}{2} + \frac{\sqrt{\Phi_0^2 - 2\Phi_0\sigma}}{2\kappa}. \tag{14}$$

III. INVERSE KLEIN TUNNELING EFFECT: TRANSMISSION OF LINEAR PLANE WAVES THROUGH AN INVERSE POTENTIAL STEP

Now it is time for us to introduce the concept of the inverse Klein tunneling effect where a plane wave is transmitted through an inverse potential step as schematically shown in Fig. 3(a). Now the inverse potential step $V(\xi) = \Phi_0 = -\beta_0 > 0$ for $\xi < 0$, and $V(\xi) = 0$ for $\xi \geqslant 0$. This inverse potential step can be mimicked by the array β_n in Eq. (1) with the profile shown in Fig. 3(b). Specifically, now $\beta_n = \beta_0 < 0$ for all waveguides with $n < 0$ (region I) and $\beta_n = 0$ for all waveguides with $n \geqslant 0$ (region II). As a result, the transverse refractive index profile of BWAs is now schematically illustrated in Fig. 3(c).

Obviously, all dispersion relations in the form of Eqs. (4) and (5) in Sec. II are still valid for the discrete model and the continuous model illustrated in Figs. 3(b) and 3(c) and Fig. 3(a), respectively. In Figs. 4(a) and 4(b) we plot the dispersion curves for the discrete and continuous models, respectively. The physical mechanism of the inverse KT effect is also schematically illustrated in Fig. 4. Now the solid curves in Fig. 4 represent the dispersion relations when $\Phi = \Phi_0$, i.e., region I in Fig. 3. Meanwhile, the dashed curves in Fig. 4 represent the dispersion relations when $\Phi = 0$, i.e., region II in Fig. 3. If an incident plane wave belonging to the *lower* miniband ω_- of the BWA traveling in region I in Fig. 3 and having the incident wave number $Q_0^i = \pi/2 + k_0^i/2$ such that $0 < Q_0^i < \pi/2$ (i.e., $-\pi < k_0^i < 0$), then this plane wave will hit the inverse potential step with the height $\Phi_0 = -\beta_0$. From now on, we use the superscript i to specifically indicate the *inverse* KT effect. If the inverse potential step is high enough ($\Phi_0 > 2\sigma$), one can observe the optical analog of the quantum relativistic inverse Klein tunneling for both continuous and discrete models. In this case, the transmitted wave will be another plane wave belonging to the *upper* miniband ω_+ of the BWA traveling in region II in Fig. 3 with a certain constant amplitude (instead of being damped) and with the transmitted wave number Q_1^i obtained from the energy conservation condition:

$$\omega_+(Q_1^i, 0) = \omega_-(Q_0^i, \Phi_0) \equiv \omega_0^i, \tag{15}$$

with the constraint $\pi/2 < Q_1^i < \pi$ to ensure a positive group velocity of the transmitted wave.

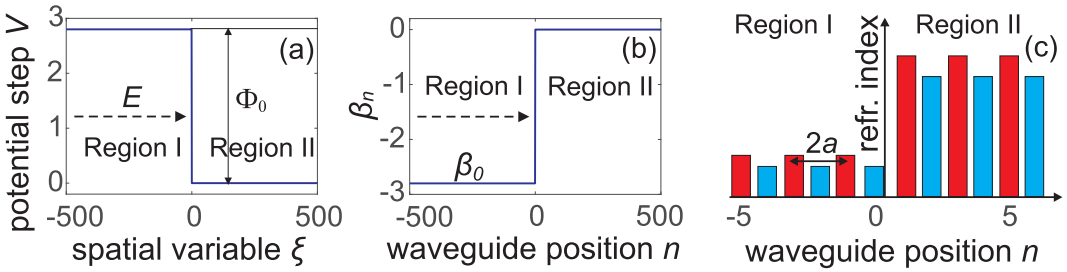

FIG. 3. (a) Scheme for investigating the inverse Klein tunneling effect of a particle with energy E through an inverse potential step $V(\xi)$ with the potential height $\Phi_0 > E$. (b) Propagation constant offset β_n introduced to a BWA to mimic the potential step $V(\xi)$. (c) Transverse refractive index profile of the BWA.

From Eqs. (6) and (15) it is easy to get the following important relationship while analyzing the KT effect and the inverse KT effect with the same potential step height Φ_0:

$$\text{if } Q_0^i = \pi - Q_0 \Leftrightarrow Q_1^i = \pi - Q_1. \tag{16}$$

As was done in Ref. [42], it is easy to show that from the dispersion relation (4) and the energy conservation law (15) the following conditions for observing the inverse KT effect in BWAs in the linear regime can be derived.

(i) If an incident plane wave hits the inverse potential step with the incident normalized wave number $0 < Q_0^i < \pi/2$, then the inverse potential step height Φ_0 must satisfy the following condition:

$$\sigma + \sqrt{\sigma^2 + 4\kappa^2 \cos^2 Q_0^i} < \Phi_0 < \sqrt{\sigma^2 + 4\kappa^2} + \sqrt{\sigma^2 + 4\kappa^2 \cos^2 Q_0^i}. \tag{17}$$

(ii) If the potential step height satisfies the condition $2\sigma < \Phi_0 < 2\sqrt{\sigma^2 + 4\kappa^2}$, then the incident wave number must satisfy the following condition (see the derivation of Eq. (15) in Ref. [42]):

$$\text{acos}\frac{\sqrt{\Phi_0^2 - 2\Phi_0\sigma}}{2\kappa} < Q_0^i < \frac{\pi}{2}. \tag{18}$$

In the continuous model, the following energy conservation relation must be held true to observe the inverse KT effect as illustrated in Fig. 4(b):

$$\epsilon_0^i \equiv \epsilon_-\left(k_0^i, \Phi_0\right) = \epsilon_+\left(k_1^i, 0\right), \tag{19}$$

with k_0^i being negative and k_1^i being positive to ensure positive group velocities for both incident and transmitted plane waves.

From Eqs. (9) and (19) it is also easy to get the following important relationship while analyzing the KT effect and the inverse KT effect with the same potential step height Φ_0 in both the continuous and discrete models:

$$\text{if } k_0^i = -k_0 \Leftrightarrow k_1^i = -k_1. \tag{20}$$

From the dispersion relation (5) and the energy conservation law (19), the following conditions for observing the inverse KT effect in the continuous model in the linear regime can be derived.

(i) If an incident plane wave hits the potential step with the incident wave number $-\pi < k_0^i < 0$, then the following condition for the inverse potential step height Φ_0 must be held true:

$$\Phi_0 > \sigma + \sqrt{\sigma^2 + \kappa^2 \left(k_0^i\right)^2}. \tag{21}$$

(ii) If the inverse potential step height satisfies the condition $\Phi_0 > 2\sigma$, then the incident wave number must satisfy the following condition:

$$-\frac{\sqrt{\Phi_0^2 - 2\Phi_0\sigma}}{\kappa} < k_0^i < 0, \tag{22}$$

or, equivalently,

$$\frac{\pi}{2} - \frac{\sqrt{\Phi_0^2 - 2\Phi_0\sigma}}{2\kappa} < Q_0^i < \frac{\pi}{2}. \tag{23}$$

By using a similar procedure (which has been developed in detail in the Appendix in Ref. [28] for deriving the analytical formula for the power transmission coefficient T in the case of the KT effect), one can get the following formula for the power transmission coefficient T^i through the inverse

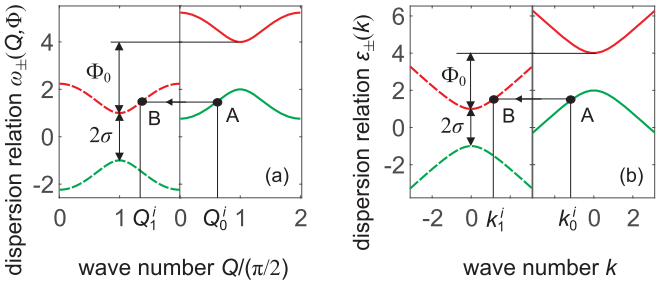

FIG. 4. (a) Dispersion relation curves $\omega_\pm(Q, \Phi)$ when $\Phi = \Phi_0$ (solid curves) and $\Phi = 0$ (dashed curves) based on Eq. (4) for explaining the physical mechanism of the inverse KT effect in BWAs in the linear regime. (b) Dispersion relation curves $\epsilon_\pm(k, \Phi)$ when $\Phi = \Phi_0$ (solid curves) and $\Phi = 0$ (dashed curves) based on Eq. (5) for explaining the physical mechanism of the inverse KT effect with the continuous model in the linear regime.

potential step in the case of the inverse KT effect:

$$T^i(Q_0^i, \Phi_0) = \frac{(\omega_0^i - \sigma - \Phi_0)(\omega_0^i - \sigma)\sin(2Q_0^i)\sin(2Q_1^i)}{\left[\Phi_0 \cos Q_0^i \cos Q_1^i\right]^2 + \left[(\omega_0^i - \sigma - \Phi_0)\sin Q_0^i \cos Q_1^i + (\omega_0^i - \sigma)\sin Q_1^i \cos Q_0^i\right]^2}. \tag{24}$$

Obviously, by analyzing Eqs. (4), (6), and (15) one can easily see that if the potential height for both the KT effect and the inverse KT effect is the same, and if $Q_0^i = Q_1$, we will have $Q_1^i = Q_0$ and $\omega_0 = \omega_0^i$. Therefore, by comparing Eqs. (7) and (24) one can easily see that in this case we have

$$T^i(Q_1, \Phi_0) = T(Q_0, \Phi_0). \tag{25}$$

Moreover, by comparing Eqs. (7) and (24), one gets the following simple important relationship if $Q_0^i = \pi - Q_0$:

$$T^i(\pi - Q_0, \Phi_0) = T(Q_0, \Phi_0). \tag{26}$$

The transmission coefficient T^i for the inverse KT effect in the form of Eq. (24) is based on Eq. (1) for the discrete model in BWAs in the *linear* regime. The transmission coefficient T_D^i for the inverse KT effect based on the Dirac Eq. (2) for the continuous model in the linear regime has the following form:

$$T_D^i(k_0^i, \Phi_0) = 1 - \left| \frac{-k_1^i(\epsilon_0^i - \sigma - \Phi_0) + k_0^i(\epsilon_0^i - \sigma)}{k_1^i(\epsilon_0^i - \sigma - \Phi_0) + k_0^i(\epsilon_0^i - \sigma)} \right|^2. \tag{27}$$

Like in the discrete KT effect with BWAs, by analyzing Eqs. (5), (9), and (19) one can easily see that if the potential height for both the KT effect and the inverse KT effect is the same, and if $k_0^i = k_1$, we will have $k_1^i = k_0$ and $\epsilon_0 = \epsilon_0^i$. Therefore, by comparing Eqs. (8) and (27) one can easily see that in this case we have

$$T_D^i(k_1, \Phi_0) = T_D(k_0, \Phi_0). \tag{28}$$

Moreover, by comparing Eqs. (8) and (27), one gets the following simple important relationship if $k_0^i = -k_0$:

$$T_D^i(-k_0, \Phi_0) = T_D(k_0, \Phi_0). \tag{29}$$

IV. INVERSE KLEIN TUNNELING EFFECT IN A BWA: SIMULATION VERSUS THEORY

In this section we numerically investigate the influence of the inverse potential step height Φ_0 and the incident wave number Q_0^i on the transmission coefficient T^i of an initial Dirac soliton. We choose DSs to examine the inverse KT effect in BWAs, because as shown in Ref. [42], one can easily create beams propagating under various angles of inclination in BWAs without distortion of their profiles. That is why DSs are excellent candidates to investigate the KT effect and the inverse KT effect in BWAs, especially when $Q_0^i \simeq \pi/2$ where it is quite problematic for Gaussian and similar beams.

In a BWA made of materials with Kerr nonlinearity and without the inverse potential step Φ_0, the analytical solution of Dirac solitons for the discrete coupled-mode Eq. (1) has been derived in Ref. [13] as follows:

$$\begin{bmatrix} a_{2n}(z) \\ a_{2n-1}(z) \end{bmatrix} = \begin{bmatrix} i^{2n} \frac{2\kappa}{w_0\sqrt{\sigma\gamma}} \mathrm{sech}\left(\frac{2n}{w_0}\right) e^{iz\left(\frac{2\kappa^2}{w_0^2\sigma} - \sigma\right)} \\ i^{2n} \frac{2\kappa^2}{w_0^2\sigma\sqrt{\sigma\gamma}} \mathrm{sech}\left(\frac{2n-1}{w_0}\right) \tanh\left(\frac{2n-1}{w_0}\right) e^{iz\left(\frac{2\kappa^2}{w_0^2\sigma} - \sigma\right)} \end{bmatrix}, \tag{30}$$

where w_0 characterizes the DS width. Although the DS in the form of Eqs. (30) propagates *parallel* to the longitudinal axis of the BWAs, it already has two central wave numbers $Q_B = \pm\pi/2$ (see Figs. 2(a) and 2(b) in Ref. [13]) corresponding to the Bragg angles $\pm\theta_B$ of the beam inclination. Therefore, as shown in Ref. [13], the DS in the form of Eqs. (30) can help to convert the discrete coupled-mode Eq. (1) into the Dirac Eq. (2) even though this DS propagates along the longitudinal axis. This is totally different from the case where a plane wave in BWAs, or more practically a Gaussian beam, is used to simulate optical analogs of quantum relativistic effects, e.g., *Zitterbewegung* [12] and the Klein tunneling effect [28,29]. In the latter case, a Gaussian beam must be launched into the BWAs under angles close to the Bragg angle. Mathematically, this means that an initial Gaussian beam in the form

$$a_n \sim \exp(-n^2/w_0^2)\exp\left[i\left(\frac{\pi}{2} + \frac{k_0^i}{2}\right)n\right] \tag{31}$$

must be used to launch into the BWAs, where k_0^i has a small value around 0, and w_0 also characterizes the Gaussian beam width.

On the contrary, in order to analyze the KT effect and the inverse KT effect with the help of a DS at the input, one needs to use the following initial condition for the DS:

$$a_n^{\mathrm{ini}} = a_n(0)\exp(ink_0^i/2), \tag{32}$$

where $a_n(0)$ in Eq. (32) is the DS solution taken at the distance $z = 0$ from Eqs. (30), and k_0^i also has a small value around 0. This initial condition in the form of Eq. (32) has been used in Ref. [42] for investigating the KT effect and will be used in the rest of this work to investigate the inverse KT effect in BWAs. We want to emphasize that in order to simulate KT one has to to take a *positive* value of k_0 as shown in Fig. 2(b), whereas for inverse KT one has to take a *negative* value of k_0^i as shown in Fig. 4(b). Note also that the initial center of DSs in the form of Eq. (32), or Gaussian beams in the form of Eq. (31), is at the center of the array with $n = 0$, but it is quite simple to transversally shift this initial beam center.

Now we analyze the influence of the inverse potential step height Φ_0 on the inverse KT effect while fixing the incident wave number $Q_0^i = 0.7\pi/2$ (i.e., $k_0^i = -0.3\pi$). In Fig. 5(a) we show the transmission coefficient T^i as a function of the inverse potential step height Φ_0 where the dotted green curve is the theoretical one based on Eq. (27) for the inverse KT effect in the continuous model; the dashed blue curve is the theoretical one based on Eq. (24) for the inverse KT effect in

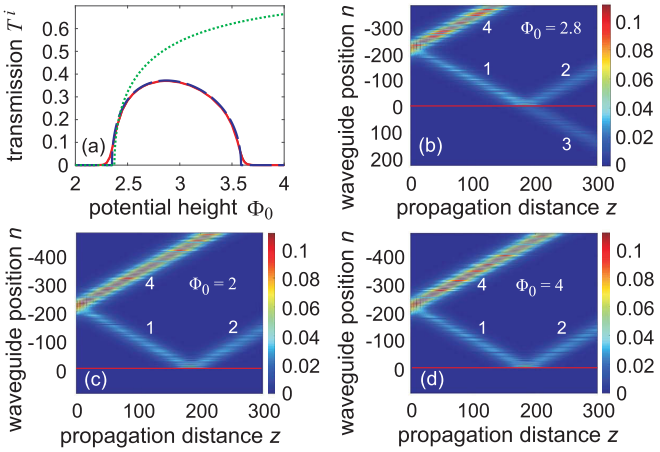

FIG. 5. (a) Transmission coefficient of DSs in BWAs as a function of the inverse potential step height: the dotted green curve is the theoretical one based on Eq. (27) for the inverse KT effect in the continuous model; the dashed blue curve is the theoretical one based on Eq. (24) for the inverse KT effect in the discrete model with BWAs; whereas the solid red curve and the green curve (hidden behind the solid red one) are obtained by the beam simulation when an initial DS is launched into the BWAs in the linear ($\gamma = 0$) and nonlinear regimes ($\gamma = 1$), respectively. (b), (c), (d) Propagation of a DS in the nonlinear regime with $\gamma = 1$, and $\Phi_0 = 2.8$, 2.0, and 4.0, respectively. Other parameters: $k_0^i = -0.3\pi$, $\sigma = 1$, $\kappa = 1$, and $w_0 = 18$.

the discrete model with BWAs; whereas the solid red curve and the green curve (hidden behind the solid red one) are obtained by the beam simulation when an initial DS with the beam width parameter $w_0 = 18$ is launched into the BWAs in the linear ($\gamma = 0$) and nonlinear regimes ($\gamma = 1$), respectively. We specially choose the large beam width parameter ($w_0 = 18$) for the initial DS to make sure that all beams in this case will be weak [see Figs. 5(b)–5(d)]; thus, even if we set $\gamma = 1$, the system will practically operate in the linear regime. As a result, two numerical curves (solid red one and green one) coincide very well with each other, and one can only see the red curve in Fig. 5(a). As clearly seen from Fig. 5(a), the theoretical dashed blue curve is in perfect agreement with the results obtained by the direct beam propagation method in BWAs and represented by the solid red curve. Therefore, the validity of Eq. (24) is confirmed.

Two theoretical curves (dotted green one and dashed blue one) in Fig. 5(a) have already been plotted in Fig. 2(a) in Ref. [42] for the KT effect under the same condition except for the incident wave number $k_0 = -k_0^i = 0.3\pi$ therein. So, the condition for Eq. (29) is fulfilled, and two theoretical curves representing T_i in Fig. 5(a) are indeed identical to the corresponding curves representing T in Fig. 2(a) in Ref. [42]. Thus, we have confirmed the validity of Eq. (29). Based on relation (17), one can easily check that for the set of parameters used in Fig. 5(a) ($\sigma = 1$, $\kappa = 1$, and $Q_0^i = 0.7\pi/2$) the theoretical condition for the inverse potential step height $2.35 < \Phi_0 < 3.59$ must be held true if one wants to observe the inverse KT effect in the discrete model with BWAs. This condition is confirmed by the dashed blue curve and the red solid curve in Fig. 5(a). Therefore, the validity of relation (17) is confirmed. In the same way, based on Eq. (21), one can easily check that for the set of parameters used in Fig. 5(a) the theoretical condition for the inverse potential step height $\Phi_0 > 2.37$ must be held true if one wants to observe the inverse KT effect in the continuous model. This condition is confirmed by the dotted green curve in Fig. 5(a). Note that two theoretical curves (dotted green one and dashed blue one) in Fig. 5(a) are almost the same if $\Phi_0 < 2.5$, but are significantly different from each other for larger values of Φ_0. This fact can be easily explained as follows. First, if $\Phi_0 < 2.35$, then the inverse potential step is not high enough for both energy conservation conditions (15) and (19) to be satisfied; thus, the inverse KT effect does not take place, i.e., the transmission coefficient is equal to 0 for these two curves. In this case, point A in Figs. 4(a) and 4(b) will be lower than the minimum points of the dashed red upper curves therein, and thus, point B cannot be found. Second, as mentioned above, the dispersion curves in the continuous model [see Eq. (5)] can only be mimicked by the dispersion curves in BWAs [see Eq. (4)] if we operate around the Dirac points, i.e., when point A is around the maximum points of the solid green lower curves and point B is around the minimum points of the dashed red upper curves in Figs. 4(a) and 4(b). This can only be satisfied if $2,35 < \Phi_0 < 2.5$. For larger values of the inverse potential step height ($\Phi_0 > 2.5$), point B in Figs. 4(a) and 4(b) will be quite far from the Dirac points, and thus, the deviation between two theoretical curves (dotted green one and dashed blue one) in Fig. 5(a) will be significant in this case.

As some examples, in Figs. 5(b)–5(d) we show the propagation process when a DS in the form of Eq. (32) is launched into the BWA in the nonlinear regime [i.e., $\gamma = 1$ for integrating Eqs. (1)] with the incident wave number being fixed $k_0^i = -0.3\pi$, and the inverse potential step height $\Phi_0 = 2.8$, 2.0, and 4.0, respectively. After launching the DS into the BWA, it is split into two beams labeled as "1" and "4" in Figs. 5(b)–5(d). Beam 1 later hits the inverse potential step (whose position at the waveguide with $n = 0$ is illustrated by the red line). In Fig. 5(b), the value $\Phi_0 = 2.8$ satisfies relation (17); therefore, we can observe the inverse KT effect in the BWA, and the incident beam 1 is divided into the reflected beam with the label 2 and the transmitted beam with the label 3. On the contrary, in Figs. 5(c) and 5(d) the values $\Phi_0 = 2.0$ and $\Phi_0 = 4.0$ cannot satisfy relation (17); therefore, we cannot observe the inverse KT effect in the BWA. As a result, after hitting the inverse potential step, beam 1 is completely reflected to form beam 2, and the transmitted beam through the inverse potential step is not generated in Figs. 5(c) and 5(d).

Now we analyze the influence of the incident wave number Q_0^i on the inverse KT effect while fixing the inverse potential step height $\Phi_0 = 2.8$. In the *left* part of Fig. 6(a) we plot the transmission coefficient T^i of the *inverse* KT effect as a function of Q_0^i where the dotted green and dashed blue curves represent the theoretical values of T^i based on Eqs. (27) and (24) in the linear case for the continuous and discrete models, respectively. Analogously, in the *right* part of Fig. 6(a) we plot the transmission coefficient T of the KT as a function of Q_0, where the dotted green and dashed blue curves represent the theoretical values of T based on Eqs. (8) and (7) in the linear case for the continuous and discrete models, respectively.

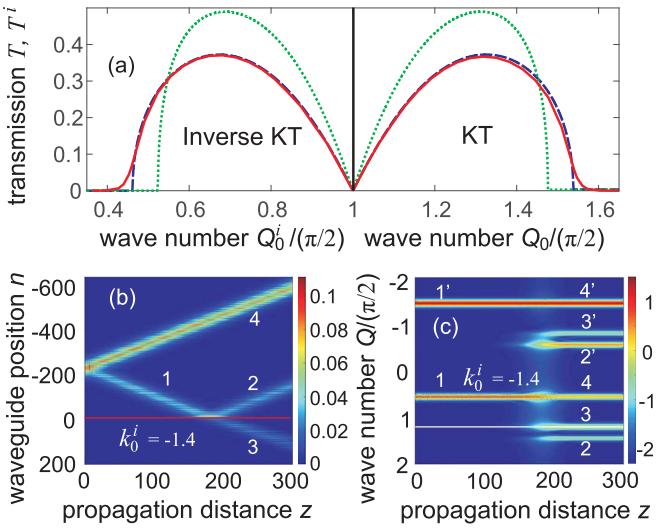

FIG. 6. (a) Transmission coefficient as a function of the incident wave number Q_0: the dotted green curve is based on Eqs. (8) and (27) for the continuous model, the dashed blue curve is based on Eqs. (7) and (24) for the discrete model, and the solid red curve is obtained by the direct beam simulation when a large DS is launched into BWAs with $\gamma = 0$. (b) Propagation of beams when a Dirac soliton is launched into BWAs in the linear regime with $\gamma = 0$ and $k_0^i = -1.4$. (c) Evolution of the spectrum in the (Q, z) plane. Other parameters: $\sigma = 1$, $\kappa = 1$, $w_0 = 18$, $\Phi_0 = 2.8$, and the array consists of 1601 waveguides.

Note that the right part of Fig. 6(a) has been illustrated like Fig. 5(a) in Ref. [42] where we have just focused on the KT effect.

From Fig. 6(a) one can easily see that the vertical black line at $Q_0 = \pi/2$ is the line of symmetry of two theoretical curves (dotted green one and dashed blue one) for the left part representing the inverse KT effect and the right part representing the KT effect. This symmetry confirms the correctness of two relationships for the inverse KT effect in the form of Eq. (26) for the discrete model in BWAs and Eq. (29) for the continuous model. Note that the dashed blue curve for the inverse KT effect in the discrete model in BWAs goes to 0 at $Q_0^i \simeq 0.46\pi/2$, which totally agrees with relation (18) when we set $\Phi_0 = 2.8$, $\sigma = 1$, and $\kappa = 1$. The dashed blue curve for the KT effect goes to 0 at $Q_0 \simeq 1.54\pi/2$, which also perfectly agrees with relation (11). Similarly, the dotted green curve for the inverse KT effect in the continuous model goes to 0 at $Q_0^i \simeq 0.52\pi/2$, which also totally agrees with relation (23). The dotted green curve for the KT effect goes to 0 at $Q_0 \simeq 1.48\pi/2$, which also perfectly agrees with relation (14).

To check the accuracy of the theoretical dashed blue curve for the KT effect and the inverse KT effect with the discrete model in BWAs, we plot the solid red curve in Fig. 6(a), which is obtained by the direct beam simulation method when a large DS ($w_0 = 18$) is launched into BWAs with $\Phi_0 = 2.8$ and in the linear regime with $\gamma = 0$. As shown in Fig. 6(a) the numerical solid red curve is in good agreement with the theoretical dashed blue curve. The only significant deviation between these two curves in Fig. 6(a) is that the solid red curve based on the direct beam simulation method smoothly goes to 0 at $Q_0^i \simeq 0.46\pi/2$ and at $Q_0 \simeq 1.54\pi/2$, whereas the theoretical dashed blue curve goes abruptly to 0 at these two points. This deviation is due to the fact that the theoretical dashed blue curve is obtained for plane waves with infinite width in BWAs, whereas the solid red curve is obtained for BWAs with finite beams widths. So, if we increase further the beam width parameter n_0 for the incident DS, these two curves will become closer and closer as already shown in Ref. [42] for the KT effect in BWAs.

As an example, in Fig. 6(b) we show the evolution of $|a_n(z)|$ when a DS is launched into BWAs in the linear regime (i.e., $\gamma = 0$) with $k_0^i = -1.4$ (thus, the incident wave number $Q_0^i = \pi/2 + k_0^i/2 \simeq 0.55\pi/2$), where the red line again indicates the position of the inverse potential step at $n = 0$. The transmission coefficient $T_i = 0.3125$ is obtained directly from the simulation by calculating the ratio of the output power (taken from the transmitted beam 3) to the input power (taken from the incident beam 1). The evolution of the Fourier transform of a_n along z is shown in Fig. 6(c). Each beam in Fig. 6(b) generates two spectrum bands with the distance between them equal to π (see also Fig. 5 in Ref. [42]). For example, the incident beam 1 in Fig. 6(b) generates two spectrum bands around $Q_0^i \simeq 0.55\pi/2$ with label 1, and $Q_0 \simeq -1.45\pi/2$ with label 1' in Fig. 6(c) (see also Figs. 2(a) and 2(b) in Ref. [13] where a DS with $k_0 = 0$ is launched into BWAs). The transmitted beam 3 in Fig. 6(b) generates two spectrum bands with labels 3 and 3' in Fig. 6(c) which are in excellent agreement with the theoretical value $Q_1^i = \pi/2 + k_1^i/2 \simeq 1.2\pi/2$ as predicted by Eq. (15) and represented by the thin white line in Fig. 6(c). So, the validity of Eq. (15) is demonstrated. Similarly, beam 4 in Fig. 6(b) generates two spectrum bands with labels 4 and 4' in Fig. 6(c). Note that the spectrum bands 1 and 4 are in the same position. This is also true for the spectrum bands 1' and 4'. This fact has been checked and proved in Ref. [42] (see Fig. 5 therein for more details).

V. CONCLUSIONS

We have systematically investigated the optical analog of the inverse Klein tunneling effect—a quantum relativistic effect—of Dirac solitons through an inverse potential step in BWAs. As it is already well known, the KT effect can be observed if an incident beam belonging to the positive branch of the dispersion relation hits the potential step and generates the transmitted beam belonging to the negative branch once the energy conservation law is fulfilled. In an opposite manner, we have shown that the inverse KT effect can be observed if an incident beam belonging to the negative branch hits the inverse potential step and generates the transmitted beam belonging to the positive branch. The transmission coefficients of a plane wave through the inverse potential step in the discrete model with BWAs and in the continuous model are obtained analytically. As expected, these two theoretical results are in good agreement with each other if we operate around the Dirac points for all the incident, transmitted, and reflected beams. The theoretical transmission coefficient in the discrete model with BWAs is in excellent agreement with

the numerical results obtained directly via the beam propagation simulation method. The influence of the inverse potential step height and the incident wave number of Dirac solitons on the inverse KT effect has been investigated systematically, which helps to confirm the validity of the theoretical transmission coefficient in the discrete model with BWAs. We have also obtained some important relations when comparing the transmission coefficients of the inverse KT effect with those of the KT effect. Our results show that Dirac solitons in BWAs are quite useful for studying the optical analogs of the KT effect, the inverse KT effect, and other quantum relativistic effects emerging from the Dirac equations.

ACKNOWLEDGMENTS

This work was funded by Vingroup and supported by the Vingroup Innovation Foundation (VINIF) under Project No. VINIF.2021.DA00001. M.C.T. is thankful to the Van Lang University.

[1] D. N. Christodoulides, F. Lederer, and Y. Silberberg, Nature (London) **424**, 817 (2003).
[2] A. L. Jones, J. Opt. Soc. Am. **55**, 261 (1965).
[3] D. N. Christodoulides and R. I. Joseph, Opt. Lett. **13**, 794 (1988).
[4] Y. S. Kivshar and G. P. Agrawal, *Optical Solitons: From Fibers to Photonic Crystals* (Academic Press, San Diego, 2003).
[5] F. Lederer, G. I. Stegeman, D. N. Christodoulides, G. Assanto, M. Segev, and Y. Silberberg, Phys. Rep. **463**, 1 (2008).
[6] Tr. X. Tran and F. Biancalana, Phys. Rev. Lett. **110**, 113903 (2013).
[7] Tr. X. Tran and F. Biancalana, Opt. Express **21**, 17539 (2013).
[8] Tr. X. Tran, D. C. Duong, and F. Biancalana, Phys. Rev. A **89**, 013826 (2014).
[9] T. Pertsch, P. Dannberg, W. Elflein, A. Bräuer, and F. Lederer, Phys. Rev. Lett. **83**, 4752 (1999).
[10] G. Lenz, I. Talanina, and C. M. de Sterke, Phys. Rev. Lett. **83**, 963 (1999).
[11] M. Ghulinyan, C. J. Oton, Z. Gaburro, L. Pavesi, C. Toninelli, and D. S. Wiersma, Phys. Rev. Lett. **94**, 127401 (2005).
[12] F. Dreisow, M. Heinrich, R. Keil, A. Tünnermann, S. Nolte, S. Longhi, and A. Szameit, Phys. Rev. Lett. **105**, 143902 (2010).
[13] Tr. X. Tran, S. Longhi, and F. Biancalana, Ann. Phys. (Amsterdam, Neth.) **340**, 179 (2014).
[14] Tr. X. Tran, X. N. Nguyen, and D. C. Duong, J. Opt. Soc. Am. B **31**, 1132 (2014).
[15] Tr. X. Tran and D. C. Duong, Ann. Phys. (Amsterdam, Neth.) **361**, 501 (2015).
[16] Tr. X. Tran, X. N. Nguyen, and F. Biancalana, Phys. Rev. A **91**, 023814 (2015).
[17] C. Koke, C. Noh, and D. G. Angelakis, Ann. Phys. **374**, 162 (2016).
[18] Tr. X. Tran, J. Opt. Soc. Am. B **36**, 2001 (2019).
[19] R. Jackiw and C. Rebbi, Phys. Rev. D **13**, 3398 (1976).
[20] Tr. X. Tran and F. Biancalana, Phys. Rev. A **96**, 013831 (2017).
[21] Tr. X. Tran, H. M. Nguyen, and D. C. Duong, Phys. Rev. A **100**, 053849 (2019).
[22] Tr. X. Tran, D. C. Duong, and F. Biancalana, J. Lightwave Technol. **35**, 5092 (2017).
[23] R. B. Laughlin, Rev. Mod. Phys. **71**, 863 (1999).
[24] M. Z. Hasan and C. L. Kane, Rev. Mod. Phys. **82**, 3045 (2010).
[25] M. C. Rechtsman, J. M. Zeuner, Y. Plotnik, Y. Lumer, D. Podolsky, F. Dreisow, S. Nolte, M. Segev, and A. Szameit, Nature (London) **496**, 196 (2013).
[26] Tr. X. Tran, J. Opt. Soc. Am. B **36**, 2559 (2019).
[27] Tr. X. Tran, Phys. Rev. A **101**, 063826 (2020).
[28] S. Longhi, Phys. Rev. B **81**, 075102 (2010).
[29] F. Dreisow, R. Keil, A. Tünnermann, S. Nolte, S. Longhi, and A. Szameit, Europhys. Lett. **97**, 10008 (2012).
[30] O. Klein, Z. Phys. **53**, 157 (1929).
[31] H. Nitta, T. Kudo, and H. Minowa, Am. J. Phys. **67**, 966 (1999).
[32] F. Sauter, Z. Phys. **69**, 742 (1931).
[33] K. S. Novoselov, A. K. Geim, S. V. Morozov, D. Jiang, M. I. Katsnelson, I. V. Grigorieva, S. V. Dubonos, and A. A. Firsov, Nature (London) **438**, 197 (2005).
[34] M. I. Katsnelson, K. S. Novoselov, and A. K. Geim, Nat. Phys. **2**, 620 (2006).
[35] S. Y. Zhou, G.-H. Gweon, J. Graf, A. V. Fedorov, C. D. Spataru, R. D. Diehl, Y. Kopelevich, D.-H. Lee, S. G. Louie, and A. Lanzara, Nat. Phys. **2**, 595 (2006).
[36] C. W. J. Beenakker, Rev. Mod. Phys. **80**, 1337 (2008).
[37] A. F. Young and P. Kim, Nat. Phys. **5**, 222 (2009).
[38] N. Stander, B. Huard, and D. Goldhaber-Gordon, Phys. Rev. Lett. **102**, 026807 (2009).
[39] G. A. Steele, G. Gotz, and L. P. Kouwenhoven, Nat. Nanotechnol. **4**, 363 (2009).
[40] R. Gerritsma, B. P. Lanyon, G. Kirchmair, F. Zähringer, C. Hempel, J. Casanova, J. J. García-Ripoll, E. Solano, R. Blatt, and C. F. Roos, Phys. Rev. Lett. **106**, 060503 (2011).
[41] O. Bahat-Treidel, O. Peleg, M. Grobman, N. Shapira, M. Segev, and T. Pereg-Barnea, Phys. Rev. Lett. **104**, 063901 (2010).
[42] Q. Nguyen-The and Tr. X. Tran, J. Opt. Soc. Am. B **37**, 1911 (2020).
[43] A. A. Sukhorukov and Y. S. Kivshar, Opt. Lett. **27**, 2112 (2002).
[44] S. Longhi, Opt. Lett. **35**, 235 (2010).
[45] W. Greiner, *Relativistic Quantum Mechanics* (Springer-Verlag, Berlin, 1990), Chap. 13.